Nature of Oxides in Al–Mg Alloys

Zhichao Niu[1] · **Shihao Wang[1]** · **Feng Gao[1]** ·
Zhongyun Fan[1]

Abstract Acting as substrates for heterogeneous nucleation, native oxides in Al–Mg alloys have shown their potential for grain refinement. However, the limited knowledge about the nature of the oxides in Al–Mg alloys impedes the widespread application as native grain refiners. The aim of this work is to comprehensively investigate the native oxides in Al–Mg alloys through electron microscopy. Our results show that the predominant inclusions in Al–Mg alloys are oxides in three types of oxide films at the micrometer scales: young films, old films and oxide skins. All oxide films consist of discrete oxide particles of three types in nanometer scale depending on the Mg contents: γAl_2O_3 (< 0.4 wt.%), $MgAl_2O_4$ (0.08–3.5 wt.%) and MgO (> 2 wt.%). Specifically, $MgAl_2O_4$ particles have sizes ranging from a few tens to a few hundreds nanometer and possess an elementary shape of octahedron faceted by {111} planes. In Al–Mg alloys, the native oxides have a lognormal size distribution, with the average mean size fluctuating in accordance with the oxide configurations as Mg content varies. The agglomerating feature causes inhomogeneous sampling, and dual-peak lognormal curves are found for low-Mg-content alloys (0.08/0.4%), which could be eliminated by increasing the Mg content (2.0/3.5%) or by using the high-shear melt conditioning (HSMC) technology. Understanding the native oxides in Al–Mg alloys shall provide instructions on their application in grain refinement.

1 Introduction

Owing to the advantageous properties of high specific strength, lightweight, corrosion resistance, recyclability and formability, aluminum alloys have been extensively used in transportation industries as potential strategies for net zero [1–4]. However, the inevitable oxidation of aluminum and its alloys during casting introduces oxide defects that deteriorate the ingot's casting integrity and mechanical properties [5–10]. The filming nature of oxides leads to the formation of re-entrapped bi-films that act as metallurgical defects detrimental to the casting performance [10]. Nevertheless, the harmful oxide films/agglomerates can be converted into beneficial factors. Recent studies have revealed by advanced electron microscopy that oxide films are comprised of discrete oxide particles, which can be applied as native nucleation sites for grain refinement after the dispersion by external forces, such as high-shear melt conditioning and ultrasonic [11–18]. From the lattice misfit point of view, native oxides, such as γ-Al_2O_3, α-Al_2O_3, $MgAl_2O_4$ and MgO, can act as the nucleating substrates for α-Al solid [19], which are comparable with some of existing grain refiners [12]. Their dispersion significantly increases the existing nucleating sites to promote grain initiation and hence grain refinement. It has been proposed that native oxides could be a sustainable grain refiner for aluminum and magnesium alloys [19, 20]. Understanding the natural features of native oxides, especially for oxide particle size and size distribution in various aluminum alloys, is becoming crucial.

This research aims to comprehensively investigate the native oxides in Al–Mg alloys and bridge the gap of

✉ Zhongyun Fan
 zhongyun.fan@brunel.ac.uk

1 Brunel Centre for Advanced Solidification Technology
 (BCAST), Brunel University London, Uxbridge, Middlesex,
 London UB8 3PH, UK

understanding between the nature of existing oxides and the grain refinement behavior. The characterization of oxides in a wide range of Al–Mg alloys either with or without high-shear melt conditioning (HSMC) is carried out to study the native oxides in terms of morphology, particle size, size distribution and their effects on grain refinement.

2 Materials preparation and experimental setup

In this work, the CPAl (99.93%) ingots were melted at 750 °C in resistance furnaces, and each set of CPMg (99.95%) was then added into the melts, respectively, and isothermally held for approximately 3 h for homogenization. The chemical compositions of Al–Mg alloys were verified by inductively coupled plasma atomic emission spectroscopy (ICP-AES) using a standard mushroom sample (ø60 × 10 mm). Intensive melt shearing was conducted via a rotor–stator high-shear device prior to casting. During HSMC, the rotor rotation speed was fixed at 4000 rpm for a predetermined period of time after immersing in the melt. To collect and facilitate direct examination of the oxide films or particles, the inclusions in Al–Mg melts were concentrated by a pressurized melt filtration technique.

The nature of oxides and other inclusions was characterized on filtered Al–Mg samples. The oxides were initially identified by X-ray diffraction (XRD) on a D8 instrument in the 2 Theta degrees from 20° to 100°. The samples were further examined by a Carl Zeiss Crossbeam 340 scanning electron microscope (SEM) equipped with an energy-dispersive X-ray spectrometer (EDS). The oxide particle sizes were measured directly from SEM images using an image-processing software Fiji ImageJ, and size distributions were analyzed via Origin afterward.

3 Results

3.1 Oxide films and particles in Al–Mg alloys

Similar to the previous results [11, 13], three types of oxide films including bi-films, old films and young films are found in Al–Mg alloys (Fig. 1).

The young oxide film is identified to be the oxidation of the Al melt on the freshly exposed melt surface for a short period of time during melt handling. The young film is a flexible liquid film, which consists of nano-sized oxide particles as shown in Fig. 2a, b. Comparing with the young films, the old oxide film is found relatively stiff as a result of a long-term oxidation of the melt surface. The coarse oxide particles in micro size form a relatively dense scull on one surface, and further oxidation of the melt underneath the scull takes place through the supply of oxygen via the cracks
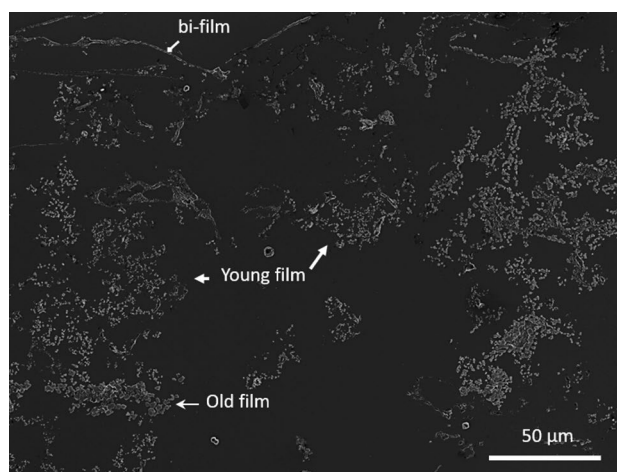

Fig. 1 SE SEM micrographs showing the morphologies of oxide films/particles including bi-films, young films and old films collected by melt filtration from Al–0.4 Mg

in the scull, forming finer oxide particles beneath the old oxide film, which is shown in Fig. 2c, d. For instance, young film and old film are identified by different dimensions of the wrinkles and folds in the form of oxide films, which consist of individual oxide particles in the Al matrix (Fig. 2). With an increase in the Mg content, the size and fraction of oxide films become relatively larger as extensive MgO films are collected in the Al–Mg melts, while the oxide particles become more discrete, together with increasing discontinuous oxide films. This is attributed to the naturally dispersed oxide particles in Al–Mg alloys containing higher Mg content [12], even without HSMC treatment.

3.2 Particle size and size distribution of oxides in Al–Mg alloys

Figure 3 shows the counted probability and size distribution of oxides in Al–Mg alloys and fitted log-normal functions. As shown in Fig. 3, dispersity promoted by HSMC treatment helps the homogeneous sampling, while it is relatively non-homogeneous for the non-HS samples. For lower Mg content (0.08 and 0.4 wt.%) Al–Mg alloys under non-HSMC, the size distributions are both fitted by two lognormal curves with different geometric mean μ, as shown in Figs. 3a, c. The dual peaks indicate that the collected oxides are from two significant groups of particle diameters: smaller/larger particles around 92/360 nm in diameter in Al-0.08 Mg and 103/510 nm in Al-0.4 Mg. For Al–Mg alloys with higher Mg content of 2.0 and 3.5 wt.%, the dual peaks are eliminated and particle size distribution becomes uniform as shown in Fig. s3 e and g. The geometric mean particle diameters are 165 nm and 135 nm for Al-2.0 Mg and Al-3.5 Mg, respectively. This means, with the increase in Mg content, the existing oxides

Fig. 2 SE SEM micrographs showing the typical morphology of oxides in Al-0.4 Mg-HS alloy: (**a**) and (**b**) show young films; (**c**) and (**d**) show old films
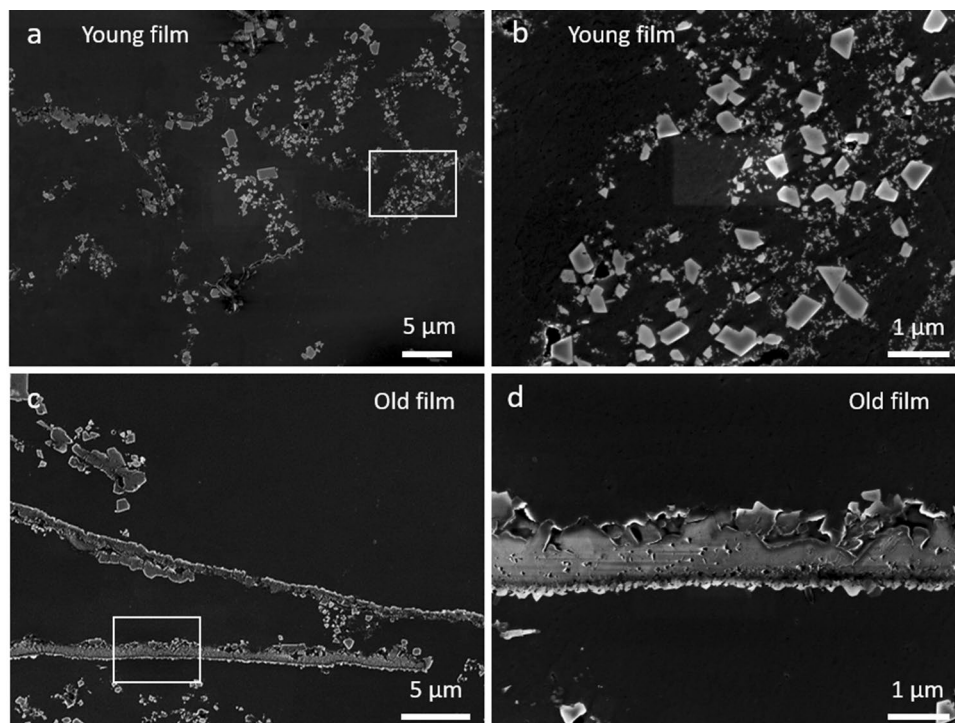
tend to be dispersed naturally and are dominated by relatively smaller particles. The standard deviation values σ at different Mg contents are all consistently around 0.5–0.7. Regarding the Al–Mg alloys under HSMC, the size distributions are uniform and fitted by a single lognormal curve for all different Mg contents, as shown in Figs. 3b, d, f, h. The geometric mean particle diameters μ are relatively smaller (68, 80, 78 and 71 nm) than those under non-HSMC (92/360, 103/510, 165 and 135 nm). The values of standard deviation σ are consistently around 0.6 for all four Al–Mg alloys. The size distribution results shown in Table 1 illustrate that the mean particle size increases with increasing Mg content from 0.08 wt.% to 0.4 wt.%, and thereafter gradually decreases with increasing Mg content up to 3.5 wt.% for both non-HSMC and HSMC. The reason is that the oxides are mainly in the form of γ-Al_2O_3 with small particle size at lower Mg content of 0.08 wt.%; when Mg content increases to 0.4 wt.%, the oxides are dominated by $MgAl_2O_4$ with relatively larger particle size; and with further increasing Mg content to 2.0 wt.% and 3.5 wt.%, the oxides are mainly presented as MgO, which normally has smaller particle size comparing to $MgAl_2O_4$.
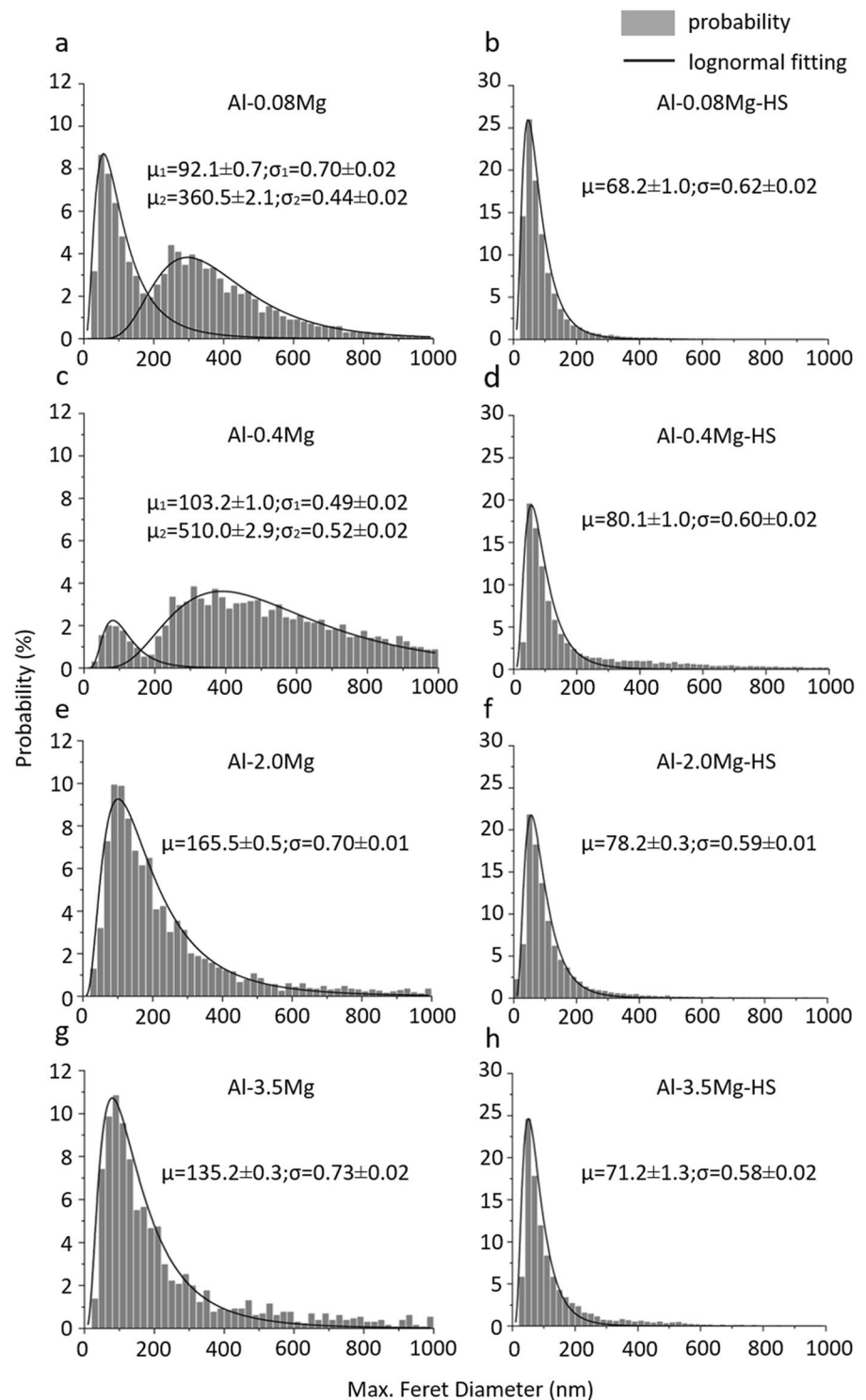
4 Discussion

The nucleation potencies of Al_2O_3 (α- and γ-) and $MgAl_2O_4$ for α-Al have been confirmed in previous research work [11, 12]. Both of these oxide particles are faceted with their closest packed {111} crystal planes, and the lattice misfits at the

interface between oxides and α-Al are comparably small. The good lattice matching at the solid/substrate interface enables the planes to provide the required substrate surfaces for heterogeneously nucleating α-Al [11, 12]. As a result, the terminating surfaces of these oxide particles existing in Al–Mg alloys are all confirmed to be potent for heterogeneous nucleation of α-Al.

In general, in order to achieve grain refinement in line with the free growth model, the potent oxides acting as nucleation substrates are desired to have a proper particle size, a narrow size distribution and also an adequate number density [21, 22]. For Al–Mg alloys in this research, only the largest nucleated particle in each oxide film can be triggered for grain initiation, which is due to the rise in solute concentration and latent heat released from the growth of initiated grain reducing the local undercooling and stopping any other smaller individual oxide particles inside the same film to achieve grain initiation [23]. The effects of different Mg contents and intensive melt shearing on the grain refinement in Al–Mg alloys have been reported in previous research work [12]. For Al–Mg alloys with lower Mg contents (0.08% and 0.4%) under non-HSMC, there are two groups of oxides with varied particle sizes and size distributions (Fig. 3) and the oxides in the melts have a poor natural dispersity. The insufficient effective number density of oxides, most of which are in the form of either films or agglomerates, limits the grain refinement efficiency, as shown in previous experimental results [12]. Nevertheless, at higher levels of Mg content in Al–Mg alloys, the naturally dispersing tendency of oxides

Fig. 3 Size distribution statistics of oxide particles in Al–Mg alloys under non-HSMC and HSMC, respectively

legend: probability ▮ ; lognormal fitting ——

a Al-0.08Mg
$\mu_1 = 92.1 \pm 0.7; \sigma_1 = 0.70 \pm 0.02$
$\mu_2 = 360.5 \pm 2.1; \sigma_2 = 0.44 \pm 0.02$

b Al-0.08Mg-HS
$\mu = 68.2 \pm 1.0; \sigma = 0.62 \pm 0.02$

c Al-0.4Mg
$\mu_1 = 103.2 \pm 1.0; \sigma_1 = 0.49 \pm 0.02$
$\mu_2 = 510.0 \pm 2.9; \sigma_2 = 0.52 \pm 0.02$

d Al-0.4Mg-HS
$\mu = 80.1 \pm 1.0; \sigma = 0.60 \pm 0.02$

e Al-2.0Mg
$\mu = 165.5 \pm 0.5; \sigma = 0.70 \pm 0.01$

f Al-2.0Mg-HS
$\mu = 78.2 \pm 0.3; \sigma = 0.59 \pm 0.01$

g Al-3.5Mg
$\mu = 135.2 \pm 0.3; \sigma = 0.73 \pm 0.02$

h Al-3.5Mg-HS
$\mu = 71.2 \pm 1.3; \sigma = 0.58 \pm 0.02$

Probability (%) — Max. Feret Diameter (nm)

leads to a more uniform size distribution (Table 1). In addition, the dramatic increase in the oxide number density results in a significant grain refinement even without intensive melt shearing [12]. Regarding the Al–Mg alloys under HSMC treatment, the dispersive power of HSMC eliminates the uneven size distribution, which leads to well-dispersed oxides with narrow size distribution but slightly smaller particle size even at lower Mg contents. The enormous oxides provide an extensive number of potent nucleation substrates for heterogeneous nucleation and grain initiation and eventually promote grain refinement. This phenomenon is not

Table 1 Quantification of oxide particle size and size distributions follow a log–normal function

	Non-HSMC		HSMC	
	μ (nm)	σ	μ (nm)	σ
Al-0.08 Mg	92.1/360.5	0.7/0.44	68.2	0.62
Al-0.4 Mg	103.2/510.0	0.49/0.52	80.1	0.60
Al-2.0 Mg	165.5	0.70	78.2	0.59
Al-3.5 Mg	135.2	0.73	71.2	0.58

so significant at high Mg contents due to the effect of self-dispersity of oxides with high Mg contents [12].

Overall, both high Mg contents and intensive melt shearing are supposed to extensively enhance the dispersity of oxides in the melts, which leads to significant grain refinement.

5 Conclusion

1. Our experiment confirmed that there are three types of oxide films in Al–Mg alloys: young films, old films and bi-films; all oxide films consist of discrete oxide particles in nanometer scale depending on the Mg contents.

2. In all Al–Mg alloys, the oxides have a lognormal size distribution. Without HSMC, the agglomerating features cause inhomogeneous sampling, and dual-peak lognormal curves are found for low-Mg-content alloys (0.08/0.4%), which can be eliminated by increasing the Mg content (2.0/3.5%) or by the HSMC treatment.

3. The average size of oxides varies with Mg content, reflecting the composition of oxide types in each Al–Mg alloy. The γ-Al_2O_3 and $MgAl_2O_4$ in Al-0.08 Mg-HSMC have an average value of 68.2 nm. The value increases to 80.1 nm due to the increasing number of $MgAl_2O_4$ and decreasing number of γ-Al_2O_3 in Al-0.4 Mg-HSMC. The gradual increase of MgO in Al-2/3.5 Mg-HSMC again drops the average value down to 78.2 nm/71.2 nm, respectively.

4. Both high Mg contents and intensive melt shearing are supposed to extensively enhance the dispersity of oxides in the melts, which leads to significant grain refinement.

References

1. Taub A I, Krajewski P E, Luo A A, and Owens J N, *JOM* **59** (2007) 48. https://doi.org/10.1007/s11837-007-0022-7
2. Benedyk J C, *Woodhead Publishing* (2010). https://doi.org/10.1533/9781845697822.1.79
3. Rowe J, Advanced Materials in Automotive Engineering. *Woodhead Publishing* (2012). https://doi.org/10.1533/9780857095466.1
4. Cann J L, et al., *Prog Mater Sci* **117** (2021) 100722. https://doi.org/10.1016/J.PMATSCI.2020.100722
5. Cabrera N, Mott N F, and Wills H H, *Rep Progr Phys* **12** (1949) 163. https://doi.org/10.1088/0034-4885/12/1/308
6. Fehlner F P, and Mott N F, *Oxid Metals* **2** (1970) 59. https://doi.org/10.1007/BF00603582
7. Schultze J W, and Lohrengel M M, *Electrochim Acta* **45** (2000) 2499. https://doi.org/10.1016/S0013-4686(00)00347-9
8. Cao X, and Campbell J, *Metall Mater Trans A* **34** (2003) 1409. https://doi.org/10.1007/s11661-003-0253-3
9. Cao X, and Campbell J, *Metall Mater Trans A* **35** (2004) 1425. https://doi.org/10.1007/s11661-004-0251-0
10. Campbell J, Castings, 2nd ed. Oxford: Elsevier, 2003. eBook ISBN: 9780080488448
11. Wang Y, Li H T, and Fan Z, *Trans Indian Inst Met* **65** (2012) 653. https://doi.org/10.1007/s12666-012-0194-x
12. Li H T, Wang Y, and Fan Z, *Acta Mater* **60** (2012) 1528. https://doi.org/10.1016/J.ACTAMAT.2011.11.044
13. Fan Z, Wang Y, Xia M, and Arumuganathar S, *Acta Mater* **57** (2009) 4891. https://doi.org/10.1016/J.ACTAMAT.2009.06.052
14. Wang Y, Peng G and Fan Z, *In Proceedings of Magnesium Technology 2017*, 99 DOI: https://doi.org/10.1007/978-3-319-52392-7_17
15. Oh J M, et al., *Mater Trans* **51** (2010) 2009. https://doi.org/10.2320/matertrans.M2010175
16. Sreekumar V M, Babu N H, and Eskin D G, *Metall Mater Trans B Process Metall Mater Process Sci* **48** (2017) 208. https://doi.org/10.1007/s11663-016-0824-5
17. Sreekumar V M, Babu N H, Eskin D G, and Fan Z, *Mater Sci Forum* **794** (2004) 155. https://doi.org/10.4028/www.scientific.net/MSF.794
18. Atamanenko T V, Eskin D G, Zhang L, and Katgerman L, *Metall Mater Trans A Phys Metall Mater Sci* **41** (2010) 2056. https://doi.org/10.1007/s11661-010-0232-4
19. Fan Z and Gao F, *Metals* **12** (2022) doi: https://doi.org/10.3390/met12101728
20. Fan Z, Gao F, Jiang B, and Que Z, *Sci Rep* **10** (2020) 1. https://doi.org/10.1038/s41598-020-66190-8
21. Greer A L, Bunn A M, Tronche A, Evans P V, and Bristow D J, *Acta Mater* **48** (2000) 2823. https://doi.org/10.1016/S1359-6454(00)00094-X
22. Quested T E, and Greer A L, *Acta Mater* **52** (2004) 3859. https://doi.org/10.1016/J.ACTAMAT.2004.04.035
23. Men H, and Fan Z, *Acta Mater* **59** (2011) 2704. https://doi.org/10.1016/J.ACTAMAT.2011.01.008

Publisher's Note Springer Nature remains neutral with regard to jurisdictional claims in published maps and institutional affiliations.